Research in Astron. Astrophys. **2010** Vol. **10** No. **4**, 309–328
http://www.raa-journal.org *http://www.iop.org/journals/raa*

***R**esearch in*
***A**stronomy and*
***A**strophysics*

Chandra archival study of (U)LIRGs with a double nucleus: binary AGNs?

Jing-Bo Wang[1,2] and Yu Gao[1]

[1] Purple Mountain Observatory, Chinese Academy of Sciences, Nanjing 210008, China; *pmogao@gmail.com*
[2] Graduate University of Chinese Academy of Sciences, Beijing 100049, China

Received 2009 July 10; accepted 2010 January 3

Abstract We present our initial results from a study of 14 (U)LIRGs with a double-nucleus (z <0.15) and an AGN signature in the *Chandra* archive. The goals of our study are to search for more possible cases of binary AGNs and to investigate the X-ray properties and energy sources of these energetic objects, a major effort devoted specifically to searching for binary AGNs from (U)LIRGs. Our studies suggest that Mrk 266 might be a new candidate in hosting binary AGNs supported by X-ray observations. Our analysis shows that most (U)LIRGs are essentially weak X-ray sources and are not dominated by AGNs, due to both the lack of Fe K line detections and weak emission in the hard X-ray band. We find evidence for thermal emission with temperature $kT\sim 0.7$ keV in seven nuclear regions, and this component is possibly associated with the nuclear or circumnuclear starburst. The soft and hard X-ray to far-infrared ratios also suggest that most (U)LIRGs are not energetically dominated by AGNs. Therefore, this study only provides one additional candidate of binary AGNs. We cannot rule out the existence of low luminosity AGNs and thus binary AGNs in all of them, particularly, those highly obscured and spatially unresolved systems. Nine of 14 (U)LIRGs, including three previously known binary AGNs and a new candidate Mrk 266, clearly have obvious X-ray counterparts to their double optical/near-IR nuclei. whereas only two out of 14 have one obvious X-ray counterpart detected. Additionally, Arp 220 and Mrk 273 are not spatially resolved owing to their small nuclear separations ($\sim 1''$), and no significant X-ray detection in the most distant source.

Key words: galaxies: active— galaxies: nuclei— infrared: galaxies— X-ray: galaxies — galaxies: individuals (Mrk 266, NGC 7592, IRAS 14348−1447, IRAS 08572+3915, II Zw 035)

1 INTRODUCTION

The presence of binary supermassive black holes (SMBHs) is thought to have wide astrophysical relevance. Binary SMBHs have been invoked to explain many astrophysical phenomena ranging from galaxy formation to various forms of activity in galaxies (Komossa et al. 2003), i.e., triggering

∗ Supported by the National Natural Science Foundation of China.

starburst and increasing AGN activity (Taniguchi & Wada 1996; Gaskell 1985), causing the difference between radio-loud AGNs (e.g., Villata & Raiteri 1999; Britzen et al. 2001), the mismatching between the orientation of radio jets and disks in AGNs (Merritt 2001, 2002), and the formation of molecular tori (Zier & Bierman 2001, 2002). Moreover, strong gravitational waves can be produced during the merging of binary BHs (Thorne & Braginskii 1976) and this phenomenon will be detected for the first time by the Laser Interferometer Space Antenna (LISA, see, i.e., Bender 1998) for BH masses in the range $\sim 10^4 - 10^7\,M_\odot$. Observations have shown that the majority of galaxies contain SMBHs in the centers of galaxies and that merging between galaxies seems to be frequent. According to the hierarchical galaxy formation model, binary BHs should be quite common (Haehnelt & Kauffmann 2002).

Several observational phenomena have pointed to the occurrence of binary SMBHs, such as X-shaped radio galaxies (e.g., Wang et al. 2003), semi-periodic signals in light curves (Valtaoja et al. 2000), helical radio patterns (Roos et al. 1993), double-double galaxies (Schoenmakers et al. 2000), galaxies which lack central cusps (Lauer et al. 2002), and double-peaked emission-line profiles (Zhou et al. 2004). However, these candidates for close SMBH pairs are still controversial, since there are alternative interpretations which do not include the existence of binary SMBHs in explaining these phenomena. Hence, it is significantly important to directly find the spatially resolved SMBH pairs of large separations in which both SMBHs can directly be identified separately.

With only a few known examples of binary BHs, however, the observational evidence of spatially resolved binary BHs has been rare until now. Luminous infrared galaxy (LIRG) merger NGC 6240 (Komossa et al. 2003) is the first unambiguous example of a binary AGN discovered by *Chandra* X-ray observations with the shortest projected distance ($\simeq$1 kpc). Later, a few cases similar to NGC 6240 with larger separations have been unveiled in X-rays, based on both *Chandra* and *XMM-Newton* observations. Such binary BHs have been claimed in LIRG merging pairs Arp 299 (IC 694/NGC 3690, Ballo et al. 2004) and Mrk 463 (Bianchi et al. 2008). Additionally, Guainazzi et al. (2005) then presented *XMM-Newton* observations of the interacting pair ESO 509-IG 066 which exhibit that both galaxies have a bright ($L_X \sim 10^{43}\,\mathrm{erg\,s^{-1}}$) and obscured X-ray nucleus. Most recently, Evans et al. (2008) reported that both the host galaxy of 3C 321 and its companion host a luminous AGN, using the multi-wavelength data from MERLIN, VLA, *Spitzer*, Hubble Space Telescope (HST), and *Chandra*.

Pairs of AGNs could be formed in the course of the merging of two galaxies, with each harboring an AGN. Ultraluminous infrared galaxies (ULIRGs) are galaxies whose infrared luminosity (8–1000 μm) exceeds $10^{12}\,L_\odot$ (Sanders & Mirabel 1996). Observations have shown that almost all ULIRGs and a significant fraction of LIRGs are undergoing interactions or mergers. Furthermore, *Chandra* X-ray observations of (U)LIRGs alone have already led to the discovery of three binary AGNs, demonstrating that X-ray is a powerful tool for exploring obscured AGNs. The energy sources of (U)LIRGs are thought to be either a powerful starburst (Joseph 1999), or an active galactic nucleus (Sanders 1999), or both. They usually have merging disks, chaotic morphologies, and often have a double-nucleus. The nature of the nuclear power source in (U)LIRGs is still uncertain, due to the large amount of dust and gas column densities in their galactic nuclei (Downes & Solomon 1998) which absorb and obscure the UV of emission of either the starbursts or AGNs, or both. It is these obscuring nuclear dust and gas that account for the infrared emission, and prevent a straightforward observation of the central energy sources. Even though there are many important diagnostics in optical and infrared spectroscopy, contradictory results have been reported about the energy source in (U)LIRGs. This emphasizes the significance of observations in X-ray, particularly the *Chandra* high spatial resolution and sensitivity, which can effectively penetrate through the obscuring materials to reveal the physical properties of the hidden nucleus.

Previous studies involving significant samples of ULIRGs in X-ray have been reported by Ptak et al. (2003), Franceschini et al. (2003), and Teng et al. (2005). The sample of Ptak et al. (2003) is a volume-limited sample and the redshifts of the galaxies do not reach above 0.045. Franceschini et al.

(2003) selected their sample from the ULIRGs in the ISO studies observed by Genzel et al. (1998) which included only the brightest nearby (U)LIRGs and the redshifts of galaxies do not exceed 0.082. Teng et al. (2005) selected from the IRAS "1 Jy sample" (Kim & Sanders 1998) to uniformly cover the *IRAS* color-luminosity plane. The case studies of several nearby LIRGs have been reported by several groups (e.g., Lira et al. 2002; Xia et al. 2002; Grimes et al. 2006; and Brassington et al. 2007).

Our sample selection encompasses more (U)LIRGs with known AGNs having lower infrared luminosities and a larger redshift range in the Chandra archive. Here we limit our sample specifically to (U)LIRGs with a known double-nucleus. In this paper, we present a *Chandra* archival study of 14 (U)LIRGs which have a double-nucleus and AGN signature revealed in other wavelengths, such as optical and near-infrared data. Section 2 discusses the sample selection and data reduction. In Sections 3 and 4, we present our results from imaging analysis and spectral modeling of the sample. Then, we discuss our results and summarize our conclusions in Sections 5 and 6, respectively. Throughout this paper, we assume the Hubble constant $H_0 = 75\,\mathrm{km\ s^{-1}\ Mpc^{-1}}$.

2 SAMPLE SELECTION AND DATA REDUCTION

In order to search for more possible cases of binary AGNs, to study the bulge-BH relation and co-evolution of AGNs and the stellar bulge of host galaxies, and to investigate the X-ray properties and energy sources of (U)LIRGs, we need a sample of (U)LIRGs with a spatially resolved double nucleus showing the AGN feature. For this purpose, we have examined the *Chandra* archival observations of (U)LIRGs and selected a total of 14 (U)LIRGs with *Chandra* ACIS observations that have a double-nucleus and an AGN signature in other wavelengths. The sources are selected by applying the following four criteria: (1) all (U)LIRGs in *Chandra* archive (2) resolvable double-nucleus in previous observations (3) redshift cut off for nearby sources (4) at least one of the nuclei of the galaxies has an AGN signature. These sources potentially provide the best candidates for harboring a double-AGN which can be found from the high sensitivity and high resolution Chandra ACIS observations.

The sample of 14 galaxies includes equal numbers of galaxies below (LIRGs) and above (ULIRGs) $10^{12}\,L_{\odot}$ with redshift between 0.01 to 0.15. Five of them are "infrared warm" ($\frac{F_{25\,\mu\mathrm{m}}}{F_{60\,\mu\mathrm{m}}} > 0.2$) and the other nine are "infrared cold" ($\frac{F_{25\,\mu\mathrm{m}}}{F_{60\,\mu\mathrm{m}}} < 0.2$). It is remarkable that virtually all of the objects in our sample are classified as galaxy mergers at different merging stages based on the multi-band observations (Veilleux et al. 2002). There are also many important spectral diagnostics in optical and infrared bands. Previously, various optical and infrared observations classified these galaxies as Seyferts, LINERs, or starbursts as can be easily checked in the NED. The Chandra observation dates, net exposure times, and some properties of these sources are listed in Table 1.

The data have been reprocessed using the *Chandra* X-ray Center (CXC) *Chandra* Interactive Analysis of Observations package (CIAO) version 4.0[1] and calibration database (CALDB) version 3.4.3 from level 1 event files. The CIAO tool acis_process_event was used to produce the new level 2 event files. In addition, the tool applies the new gain map in the CALDB and ACIS charge transfer inefficiency (CTI) correction. After a new level 2 file is produced, we apply the standard grade filtering to the data, including only the event grades 0, 2, 3, 4, and 6 (the ASCA standard grade set). Finally, we examine the background light curves, and periods of high background flares are removed when the background count rate deviates by more than 5 σ above the mean value.

X-ray images are smoothed using the CIAO adaptive smoothing task *csmooth* at the 3σ level and a maximum scale of 10 pixels to avoid over smoothing. HST optical and near-infrared images are obtained from the Multi-mission Archive at STScI and processed with the On-the-Fly Reprocessing

[1] *http://cxc.harvard.edu/ciao/*

Table 1 Basic Data for the (U)LIRG Sample

Source Name	RA (J2000)	Dec (J2000)	z	$\log_{10}\left(\frac{L_{\rm IR}}{L_\odot}\right)$	Observ. Date	Exposure[a] (ks)	$\log_{10}\left(\frac{F_{25\,\mu\rm m}}{F_{60\,\mu\rm m}}\right)$	Galactic $N_{\rm H}$ (10^{20} cm^{-2})
(1)	(2)	(3)	(4)	(5)	(6)	(7)	(8)	(9)
Arp 220	15 34 57.1	+23 30 11	0.018	12.21	06/24/2000	55.9	–1.11	4
Arp 299	11 28 30.4	+58 34 10	0.010	11.88	07/13/2001	24.2	–0.66	1
IRAS 00188−0856	00 21 26.5	−08 39 26	0.128	12.33	09/04/2003	9.7	–0.84	3
IRAS 03521+0028	03 54 42.2	+00 37 03	0.152	12.45	01/26/2006	9.5	–1.10	1
IRAS 08572+3915	09 00 25.4	+39 03 54	0.058	12.11	09/04/2003	9.8	–0.73	2
IRAS 14348−1447	14 37 38.3	−15 00 23	0.082	12.30	09/04/2003	14.8	–0.84	7
Mrk 266	13 38 17.5	+48 16 37	0.027	11.49	11/02/2001	19.5	–0.83	2
Mrk 273	13 44 42.1	+55 53 13	0.038	12.14	04/19/2000	44.0	–0.97	1
Mrk 463	13 44 42.1	+55 53 13	0.050	11.77	06/11/2004	49.2	–0.12	4
NGC 6240	16 52 58.9	+02 24 03	0.024	11.85	07/29/2001	36.6	–0.81	6
NGC 7592	23 18 22.2	−04 25 01	0.024	11.33	10/15/2006	14.9	–0.91	4
PKS B1345+125	13 47 33.3	+12 17 24	0.121	12.28	02/24/2000	25.3	–0.46	2
VV 114	01 07 47.2	−17 30 25	0.020	11.71	10/20/2000	59.1	–0.80	1
III Zw 035	01 44 30.5	+17 06 05	0.027	11.56	02/24/2006	12.8	–1.10	5

[a] The background flaring time period has been removed.

NOTE: Units of right ascension are hours, minutes, and seconds, and units of declination are degrees, arcminutes, and arcseconds.

Mazzarella, J. M., Gaume, R. A., Aller, H. D., & Hughes, P. A. 1988, ApJ, 333, 168

Positions and redshifts were taken from NED. IR luminosity and fluxes were obtained from Sanders et al. (2003) and Kim & Sanders (1998).

Galactic $N_{\rm H}$ values were obtained from Dickey & Lockman (1990) using the LHEASOFT nh tool.

(OTFR) system. These objects are observed with ACS, WFPC2, NICMOS, and with different optical and near-infrared filters. The cosmic rays are identified and removed using the IRAF[2] tasks cosmicrays and imedit. Bad columns and hot pixels are fixed by the fixpix task which substitutes them using a linear interpolation of surrounding pixels.

Spectra of each nucleus are extracted respectively using the CIAO tool psextract. The psextract tool groups spectra to a defined minimum number of counts for each bin. Associated responses are produced using the CIAO routines mkacisrmf and mkarf. We also extract the spectra of global regions which completely cover the X-ray emissions of the galaxies with the CIAO routine specextract. XSPEC package version 12.3[3] (Arnaud 1996) is used in the analysis of the spectra. We extract background spectra from a circular, source-free area adjacent to the sample galaxies on the same ACIS chip. In order to use the χ^2 statistics, the spectra are binned to have at least 15 counts in each energy channel. Channels below 0.3 keV and above 8.0 keV are neglected because the instrument calibration is uncertain at energy lower than 0.3 keV and there are few counts above 8.0 keV. For those faint sources that do not have enough counts of photons for performing the conventional spectral fitting, the hardness ratios are computed using the counts in a soft band (0.5–2.0 keV) and a hard band (2.0–8.0 keV). Then, we compare the hardness ratios with MEKAL and power-law models. This method is used to evaluate the spectral parameters of the source nuclei with less than 100 total counts. Owing to only a few number of counts detected from these faint galaxies or very limited exposure time available, we cannot apply more complex models to calculate more meaningful constraints.

[2] The Image Reduction and Analysis Facility (IRAF) is distributed by the IRAF programming group at the National Optical Astronomy Observatories (NOAO) in Tucson, Arizona. NOAO is operated by the Association of Universities for Research in Astronomy, Inc. under cooperative agreement with the National Science Foundation. IRAF version 2.14 was used in this study.

[3] *http://heasarc.gsfc.nasa.gov/docs/xanadu/xspec/*

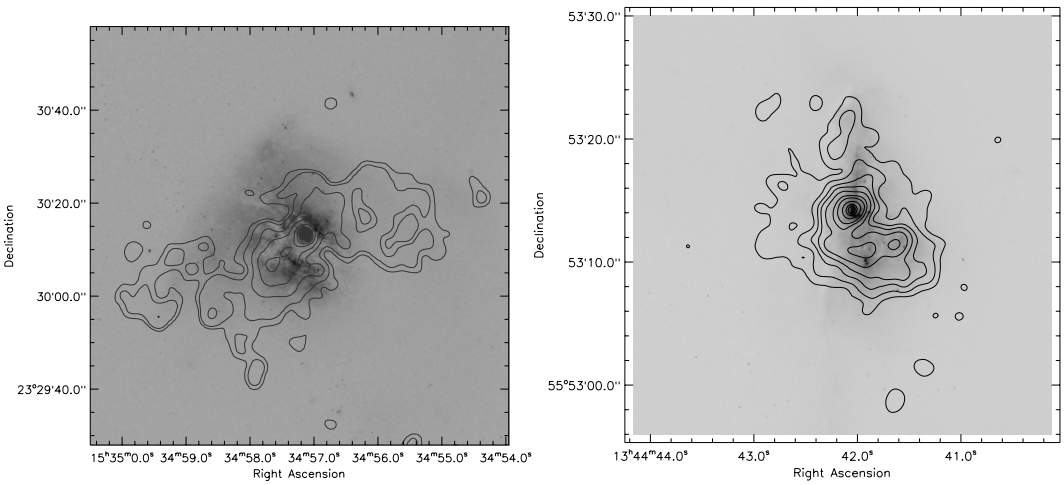

Fig. 1 Contours of 0.3–1.0 keV X-ray data of Arp 220 (*left*) and Mrk 273 (*right*) from Chandra ACIS-S overlaid on optical images from the HST. The mean background are 0.003 and 0.004 counts per pixel for the left and right panels, respectively. Contours are corresponding to 0.016, 0.024, 0.04, 0.12, 0.2, 0.28, 0.4, 0.8, 1.2, 2.0, and 2.8 counts per pixel for Arp 220. The contours of Mrk 273 are corresponding to 0.07, 0.15, 0.25, 0.35, 0.50, 0.76, 1.0, 1.5, 2.0, 2.5, 2.7, and 3.0 counts per pixel.

3 IMAGING ANALYSIS

We first compare the positions of X-ray sources with the positions of optical and near-infrared images. The offsets between X-ray peaks and infrared or optical peaks are typically $\lesssim 1''$, which are in agreement with the expected errors of measurements in these wavebands. Nine galaxies in this sample clearly have both X-ray counterparts to their double optical or near-IR nuclei. The X-ray positions of *Chandra* observations coincide with those of the HST optical and near-infrared observations within $\sim 1''$. We shift the midpoints of optical and near infrared positions between the two nuclei to match those positions of the X-ray midpoints in all figures presented in Figures 1–6 whenever necessary.

Figures 1 and 2 show the soft X-ray (0.3–1.0 keV) contours of Arp 220 and Mrk 273 and hard X-ray (2.0–8.0 keV) contours of Mrk 463 and Mrk 266 overlaid on the HST optical images, respectively. These serve as a demonstration of our imaging analysis as compared with previously published results and they are all consistent with previous studies (Xia et al. 2002; McDowell et al. 2003; Brassington et al. 2007; Bianchi et al. 2008). The double-nucleus of both Arp 220 and Mrk 273 is essentially unresolved in X-ray, thus we have simply used the same X-ray positions (the peak of X-ray emissions) for both nuclei. Mrk 266 contains two hard X-ray nuclei, a Seyfert 2 to the south and a LINER to the north (Mazzarella et al. 1988). However, the northern LINER nucleus is much brighter than the southern Seyfert 2 nucleus in X-ray. This could be a good candidate for a double-AGN though there is no direct indication of an AGN in the 0.3–10 keV band from the spectral analysis (next sub-section).

The rest of the images (Figs. 3–5, except for the last one in Fig. 6) show the X-ray contours of galaxies for the first time as they have not been previously published. Figure 3 shows soft and hard X-ray contours of NGC 7592 superimposed on the HST optical and near-infrared images. The X-ray peaks of NGC 7592 are possibly coincident with the locations of near-infrared peaks, after the small position shift $\sim 1''$ has been applied. However, there is a chance that the true eastern

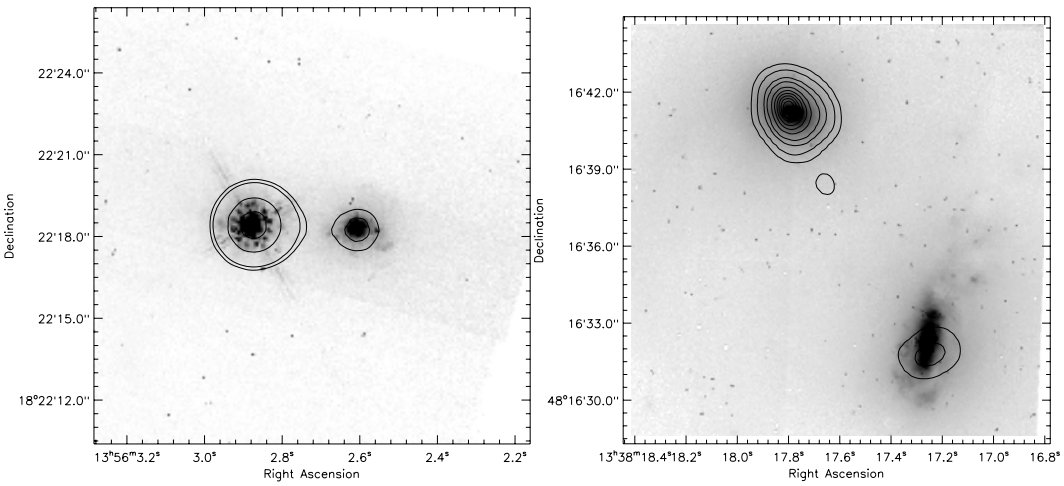

Fig. 2 Contours of 2.0–8.0 keV X-ray data of Mrk 463 (*left*) and Mrk 266 (*right*) from Chandra ACIS-S overlaid on near-infrared images from the HST. The mean background are 0.004 and 0.006 counts per pixel for the left and right panels, respectively. Contours are corresponding to 0.24, 0.40, 0.80, 2.4, 4.0, and 5.6 counts per pixel for Mrk 266. The contours of Mrk 463 are corresponding to 4.1, 7.0, 12.2, 16.3, and 20.2 counts per pixel.

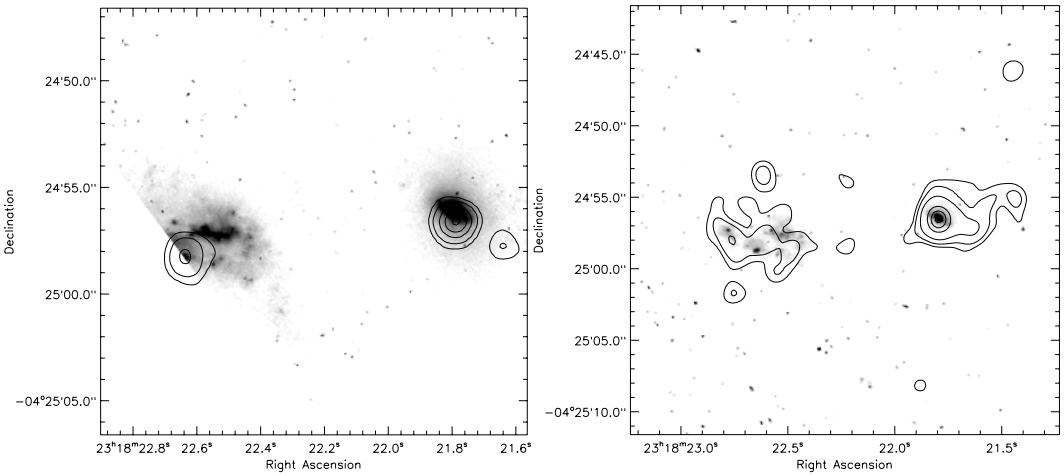

Fig. 3 Soft (*left*) and hard (*right*) X-ray contours of NGC 7592 derived from the Chandra ACIS data superimposed on the HST NICMOS images. The mean background is 0.002 counts per pixel for the left and right panels. Contours are corresponding to 0.07, 0.12, 0.25, 0.74, 1.2, and 1.8 counts per pixel for the left. The contours of the right panel are corresponding to 0.07, 0.12, 0.19, 0.27, and 0.38 counts per pixel.

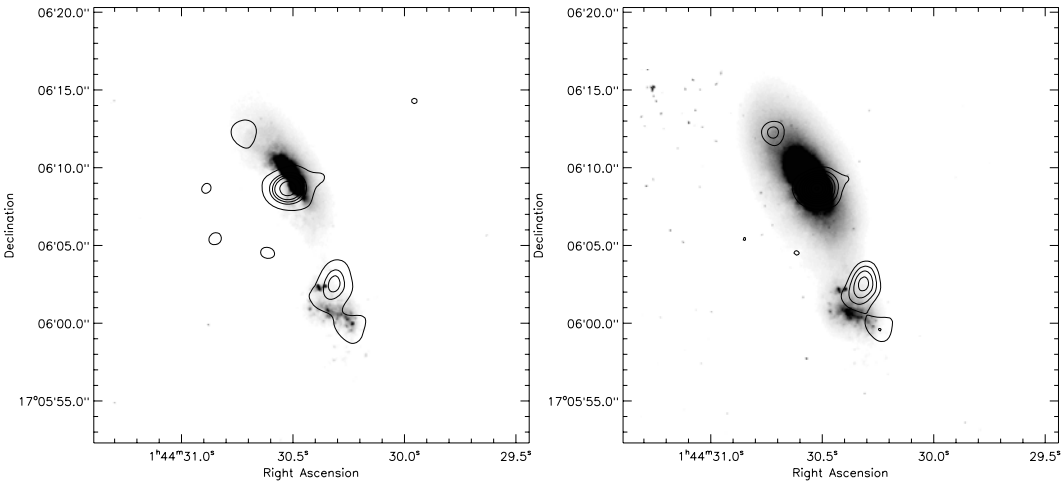

Fig. 4 HST ACS B_{435} and I_{814} bands images of III Zw 035 (*from left to right*). X-ray (0.3–8.0 keV) contours have been overlaid. The mean background is 0.004 counts per pixel. The contours are corresponding to 0.05, 0.15, 0.25, 0.34, and 0.49 counts per pixel.

nucleus (NGC 7592 E) is located just outside the FOV of the NICMOS because of the NICMOS aperture location offset (Rossa et al. 2007). We note the offset between the peaks of X-ray and HST optical images of NGC 7592 E is within 1 $''$. There is also the possibility that the X-ray peaks indeed have some small offsets from the near-infrared peaks. It is not surprising that the western nucleus of NGC 7592 is brighter in X-ray than the eastern one: the western nucleus is classified as a Seyfert 2 galaxy and the eastern one is classified as a starburst (Dopita et al. 2002). The eastern nucleus, which has little emission in either the soft X-ray or hard X-ray bands, may either be heavily obscured and absorbed or simply be extremely weak in X-ray emission.

Figure 4 shows HST ACS images at the B_{435} (left) and I_{814} (right) bands for III Zw 035 with the X-ray contours overlaid. As shown in Figure 4, the northern galaxy core of III Zw 035, classified as a type 2 Seyfert or LINER galaxy (Veilleux et al. 1995; Zink et al. 2000), is comparable in X-ray emission to the southern one which is classified as an H II nucleus.

X-ray contours overlaid on optical and near-IR images of IRAS 08572+3915 and PKS B1345+125 are shown in Figures 5 and 6, respectively. The X-ray emission of IRAS 08572+3915 is centered in the northwestern nucleus of the interacting pair, while no X-ray emission is obviously related to the southeastern one. Besides, the northwestern LINER (Veilleux et al. 1995) nucleus is unresolved (Scoville et al. 2000) and is much more luminous in all the three near-IR bands relative to the southeastern one. As can be seen from Figure 6, the X-ray emission of PKS B1345+125 is concentrated on the northwestern Seyfert 2 nucleus. However, we have not found any published references in the literature related to the spectral types for the other nucleus of these two galaxies.

Both IRAS 00188−0856 and IRAS 08572+3915 have only one component of the double-nucleus detected in X-ray. Both of these two galaxies have been classified as LINER objects (Veilleux et al. 1999), which are presumably associated with the X-ray sources that are detected here. These two galaxies have already been observed by the XMM-Newton, and the observations of XMM-Newton should give much better constraints on the existence of their AGNs. IRAS 03521+0028 is not detected in X-ray though we still keep a position to the eastern nucleus.

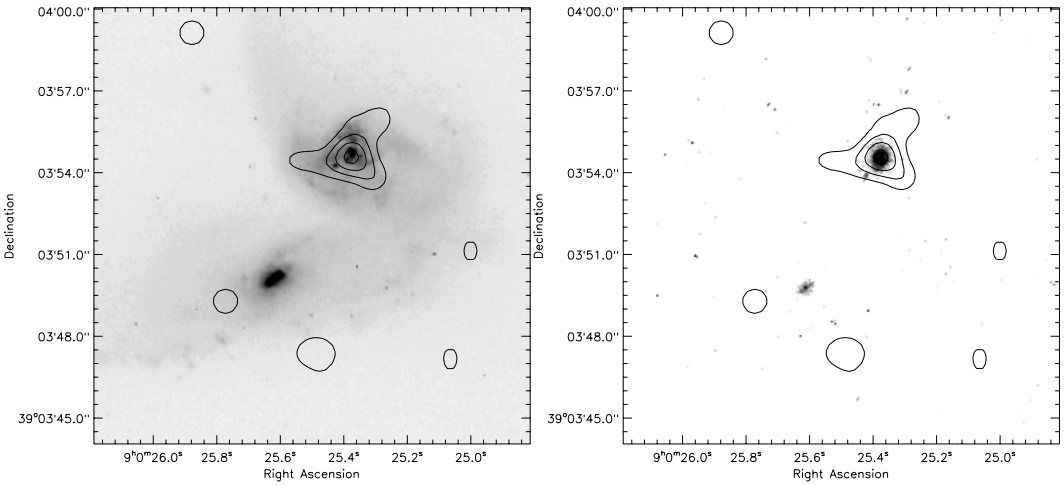

Fig. 5 HST ACS B_{435} and NICMOS K bands images of IRAS 08572+3915 (*from left to right*) with X-ray (0.3–8.0 keV) contours overlaid. The mean background is 0.006 counts per pixel. The contours are corresponding to 0.016, 0.048, 0.081, 0.11, and 0.16 counts per pixel.

These galaxies have few counts of X-ray photons and we do not try to show their X-ray morphologies given the low significance levels of photon count statistics. For example, though there are a few counts in the western nucleus of IRAS 00188−0856 and the eastern nucleus of IRAS 03521+0028, the X-ray emission of these two sources appears to be lower than the 3 σ detection level.

The X-ray emission of the double-nucleus for IRAS 14348−1447 is detected in both nuclei and they are comparable. There is no previously published X-ray image for this galaxy, but there is also not an exact spectral type reference for each nucleus of IRAS 14348–1447 in literature. This galaxy has simply been designated as a LINER object (Veilleux et al. 1999, 1997). Le Floc'h et al. (2002) found a continuum bump at 5–6 μm in VV 114 E which is a typical spectral characteristic of an AGN. Here we found that VV 114 E is much more luminous than VV 114 W in the 2–8 keV band, though the total counts of the two sources are comparable, similar to Grimes et al. (2006). The Chandra observation of NGC 6240 has been reported by Komossa et al. (2003). In addition, several papers have already presented various X-ray observations in Arp 299 (Della Ceca et al. 2002; Ballo et al. 2004; Zezas et al. 2003). Therefore, we do not show these X-ray images here.

4 SPECTRAL ANALYSIS

4.1 The Bright Sources

For nuclear sources with more than 100 counts, we have fitted these spectra with XSPEC. We initially model the nuclear spectra with a single absorbed power-law. However, these fits result in large χ^2/dof (> 1.5). We later use more complicated models to try to fit each spectrum with two or three components. The continuum of the nuclear spectra can be reproduced by a single power-law or the combination of a MEKAL or power-law and a hard power-law. Then one or two Gaussian features may be added to the continuum to account for line emission.

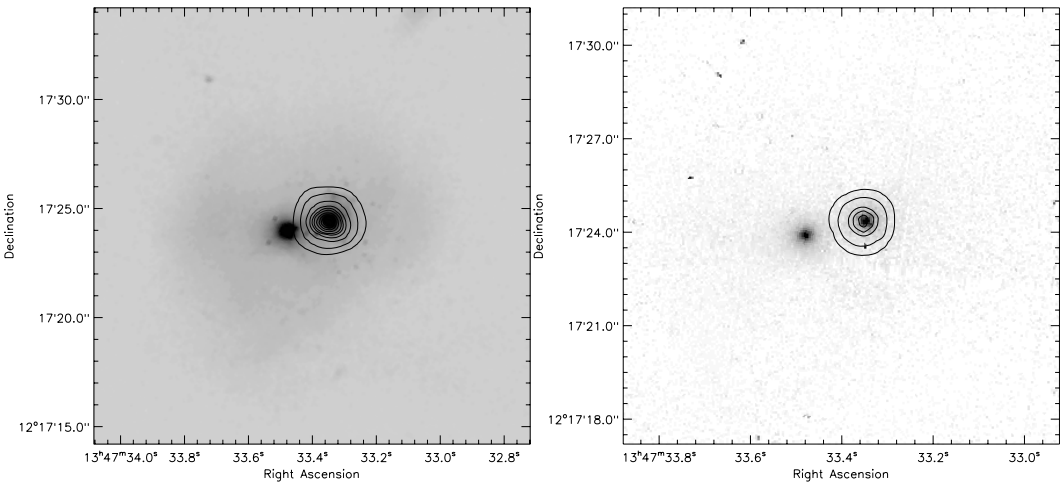

Fig. 6 HST ACS I_{814} and NICMOS H bands images of PKS B 1345+125 (*from left to right*) with soft (*left*) and hard (*right*) X-ray contour overlaid. The mean background are 0.007 and 0.012 counts per pixel. Contours are corresponding to 0.23, 0.40, 0.71, 2.38, 7.15, 11.9, 16.7, and 23.8 counts per pixel for the left. The contours of the right panel are corresponding to 2.7, 9.1, 27.4, 45.7, and 64.0 counts per pixel.

In these fits, absorption is applied to the thermal and power-law components respectively. The abundance is set to be free to be varied firstly. If the abundance is not constrained by the data, then it is fixed at solar value. The abundance is fixed at solar value in six cases (Arp 220, Mrk 266 NE, Mrk 273, Mrk 463 E, Mrk 463 W, NGC 6240 SW) and free to be varied in two cases (VV 114 E and VV 114 W). Strong Fe K emission is present in the nuclear region of Mrk 273, the double-nucleus of NGC 6240, and the eastern nucleus of Mrk 463. Since the hard X-ray continua are generally very weak, the upper limit on the equivalent width (EW) of Fe-K cannot be well constrained. However, we can determine an upper limit to the Fe-K flux and luminosity based on the background level at 6.4 keV (Ptak et al. 2003). The upper limits of the Fe-K line luminosity are usually on the order of 10^{39} erg s^{-1} or even lower, which are much smaller than typical Seyfert 2 galaxies. Some emission lines are also required for several sources (Si XIV at 3.766 keV, Fe XXI at 1.3885 keV, Fe XXI at 1.3885 keV, Ni XXI at 0.952 keV, OVIII at 0.775 keV). All these fits have $\chi^2/\mathrm{dof} < 1.3$. The results of the spectral fitting are listed in Table 2.

Our spectral fits show that the X-ray emission in these (U)LIRGs is usually not absorbed by large $N_{\rm H}$ (e.g., in excess of 10^{23} cm^{-2}). Similar fitting results have been achieved in previous work (e.g., Ballo et al. 2004 and Komossa et al. 2003) including some of the negative power-law index. Note that the column density of $N_{\rm H}$ we derived from spectral fitting is an average value over the large aperture (≥ 1 kpc), the actual value of column density over the tiny area around AGN can be extremely high. On many occasions, only hard X-ray observations (> 10 keV, such as BeppoSAX and Suzaku) can better reveal this correctly and give a reasonable $N_{\rm H}$ value. Apparently, spectral fits from either *Chandra* or XMM-Newton fail to truly unveil the high column density. In these cases where the power-law photon index is much smaller than 1.8 or even negative, strong absorption is generally suggested which is presumably a strong X-ray absorption in AGN. These are simply due to the small number statistics of hard X-ray photons collected and the photon index of the power-law spectrum cannot be well constrained by spectral fitting.

Table 2 Spectral Fits to Nuclear Regions

Parameter	Arp 220	Arp 299 E	Arp 299 W	Mrk 266 SW	Mrk 266 NE	Mrk 273	Mrk 463 E	Mrk 463 W	NGC 6240 NE	NGC 6240 SW	PKSB1345+125 NW	VV 114 E	VV 114 W
(1)	(2)	(3)	(4)	(5)	(6)	(7)	(8)	(9)	(10)	(11)	(12)	(13)	(14)
$N^a_{\rm H,1}$	$0.04^{+0.11}_{-0.0}$	—	—	—	$0.07^{+0.12}_{-0.0}$	$0.03^{+0.10}_{-0.0}$	$0.06^{+0.07}_{-0.02}$	$0.79^{+0.06}_{-0.05}$	—	$1.05^{+0.09}_{-0.07}$	—	$0.14^{+0.03}_{-0.02}$	$0.49^{+0.19}_{-0.12}$
kT (keV)	$0.75^{+0.08}_{-0.11}$	—	—	—	$0.66^{+0.05}_{-0.04}$	$0.70^{+0.04}_{-0.03}$	$0.66^{+0.02}_{-0.04}$	$0.48^{+0.06}_{-0.04}$	—	$0.94^{+0.13}_{-0.10}$	—	$0.23^{+0.01}_{-0.01}$	$0.64^{+0.15}_{-0.12}$
Z_1 ($/Z_\odot$)	1.0(f)	—	—	—	1.0(f)	1.0(f)	—	1.0(f)	1.0(f)	1.0(f)	—	$0.02^{+0.01}_{-0.01}$	$0.57^{+0.15}_{-0.12}$
K^b_M	$0.24^{+0.06}_{-0.06}$	—	—	—	$1.2^{+0.1}_{-0.09}$	$6.6^{+2.0}_{-3.3}$	$0.97^{+0.07}_{-0.07}$	$4.6^{+0.8}_{-0.8}$	—	$11.1^{+1.3}_{-1.3}$	—	$28.6^{+3.9}_{-3.9}$	$0.99^{+0.31}_{-0.30}$
$N^a_{\rm H,2}$	$1.1^{+0.21}_{-0.27}$	$0.24^{+0.15}_{-0.12}$	$0.05^{+0.20}_{-0}$	$0.26^{+0.07}_{-0.12}$	$0.07^{+0.25}_{-0.0}$	$0.75^{+0.11}_{-0.09}$	$0.08^{+0.01}_{-0.01}$	$15.38^{+2.1}_{-1.8}$	$74^{+8.5}_{-7.2}$	$0.09^{+0.48}_{-0.00}$	$3.30^{+0.25}_{-0.21}$	$2.8^{+0.08}_{-0.06}$	$1.70^{+0.63}_{-0.32}$
Γ_1	$1.1^{+0.09}_{-0.1}$	$1.0^{+0.13}_{-0.11}$	$4.8^{+0.21}_{-0.25}$	$2.1^{+0.14}_{-0.12}$	$-0.1^{+0.1}_{-0.9}$	$2.5^{+0.27}_{-0.22}$	$1.5^{+0.13}_{-0.11}$	$0.7^{+0.09}_{-0.08}$	$-2.1^{+0.2}_{-0.06}$	$-0.32^{+0.09}_{-0.08}$	$1.6^{+0.05}_{-0.04}$	$4.2^{+0.2}_{-0.17}$	$0.80^{+0.12}_{-0.18}$
$K^d_{\rm PL1}$	$0.76^{+0.08}_{-0.09}$	$1.0^{+0.13}_{-0.14}$	$1.3^{+0.16}_{-0.16}$	$1.1^{+0.16}_{-0.14}$	$0.5^{+0.7}_{-0.5}$	$3.4^{+0.39}_{-0.37}$	$1.5^{+0.2}_{-0.2}$	$1.8^{+0.2}_{-0.2}$	$0.07^{+0.02}_{-0.02}$	$0.24^{+0.03}_{-0.03}$	$20.4^{+1.3}_{-1.3}$	$23.4^{+3.0}_{-3.0}$	$0.27^{+0.26}_{-0.03}$
$N^a_{\rm H,3}$	—	—	—	—	—	—	—	—	$0.79^{+0.13}_{-0.11}$	—	$0.09^{+0.08}_{-0.06}$	—	—
Γ_2	—	—	—	—	—	—	—	—	$1.1^{+0.09}_{-0.08}$	—	$1.4^{+0.58}_{-0.39}$	—	—
$K^b_{\rm PL2}$	—	—	—	—	—	—	—	—	$2.1^{+0.17}_{-0.17}$	—	$0.80^{+0.14}_{-0.14}$	—	—
Line1 E (keV)	—	$2.38^{+0.07}_{-0.06}$	$2.51^{+0.13}_{-0.14}$	$0.90^{+0.04}_{-0.08}$	—	$6.35^{+0.12}_{-0.13}$	$0.81^{+0.03}_{-0.03}$	$1.1^{+0.22}_{-0.25}$	$6.36^{+0.02}_{-0.02}$	$6.41^{+0.04}_{-0.04}$	—	$0.92^{+0.01}_{-0.01}$	—
Line1 σ (keV)	—	$0.06^{+0.16}_{-0.06}$	$0.58^{+0.09}_{-0.09}$	$0.08^{+0.08}_{-0.04}$	—	$1.3^{+0.11}_{-0.11}$	$0.24^{+0.02}_{-0.03}$	$0.20^{+0.03}_{-0.04}$	$0.08^{+0.07}_{-0.03}$	$0.08^{+0.06}_{-0.05}$	—	$0.03^{+0.01}_{-0}$	—
$K_{\rm line1}$	—	$0.29^{+0.17}_{-0.15}$	$0.61^{+0.16}_{-0.16}$	$0.18^{+0.06}_{-0.07}$	—	$0.73^{+0.14}_{-0.21}$	$0.66^{+0.23}_{-0.15}$	$0.31^{+0.03}_{-0.05}$	$1.1^{+0.22}_{-0.26}$	$0.7^{+0.2}_{-0.2}$	—	$1.7^{+0.3}_{-0.3}$	—
Line2 E (keV)	—	$1.39^{+0.04}_{-0.05}$	—	—	—	—	$6.24^{+0.18}_{-0.16}$	—	—	—	—	—	—
Line2 σ	—	$0^{+0.10}_{-0.00}$	—	—	—	—	$1.2^{+0.15}_{-0.17}$	—	—	—	—	—	—
$K^c_{\rm line2}$	—	$0.1^{+0.1}_{-0.1}$	—	—	—	—	$2.2^{+0.27}_{-0.27}$	—	—	—	—	—	—
χ^2/dof	26.7/25	6.5/7	10.6/13	4.6/4	18.5/16	60.7/55	59.2/58	26.5/28	38.8/32	42.4/58	13.3/16	22.3/19	46.2/38

[a] $N_{\rm H}$ column densities in units of 10^{22} cm^{-2}.

[b] The normalization of the MEKAL thermal plasma model in units of $\frac{10^{-14}}{4\pi D^2}\int n_{\rm e} n_{\rm H} dV$ where D is the luminosity distance (cm) to sources, and $\rm n_e$ and $\rm n_H$ are the electron and hydrogen densities (cm^{-3}), respectively.

[c] The power-law normalization in units of 10^{-5} photons cm^{-2} s^{-1} keV^{-1} at 1 keV.

[d] The Gaussian line normalization in units of 10^{-5} photons cm^{-2} s^{-1}.

Note: All errors on spectral modeling are given as 3σ for one interesting parameter. An f indicates, the parameter was frozen at the value shown. The model fitted to the spectra was: Absorption($N_{\rm H,1}$) × Mekal(kT, Z, K_M) + Absorption($N_{\rm H,2}$) × [PL(Γ_1, $K_{\rm PL1}$) + Gaussian(E_1, σ_1, $N_{\rm Line,1}$)] + Absorption($N_{\rm H,3}$) × [PL(Γ_2, $K_{\rm PL2}$) + Gaussian(E_2, σ_2, $N_{\rm Line,2}$)], with Mekal=thermal plasma, PL = power law and Gaussian = Gaussian components.

In seven nuclear cores (Arp 220, Mrk 266 NE, Mrk 273, Mrk 463 E, Mrk 463 W, NGC 6240 SW, VV 114 W) we find the signature for thermal emission from hot plasma with a temperature $kT\sim$ 0.7 keV dominating the X-ray emission under $\sim$ 1 keV. These are consistent with the X-ray spectroscopy of local starburst galaxies, and therefore, suggest them to be possibly associated with a nuclear or circumnuclear starburst (Franceschini et al. 2003) rather than an AGN. Note that there is also a thermal component in the eastern nucleus of VV 114 with $kT\sim$ 0.23 keV, whereas Ptak et al. (1999) found that starburst galaxies usually have a temperature greater than 0.6 keV. The low temperature here indicates that the starburst activity may not be as violent as those found in a typical starburst galaxy. The power-law component dominates the X-ray emission above $\sim$ 2 keV, but the photon indexes of the power-law component vary in a large range. In order to determine the flux extended beyond the nuclear core, we extract the spectra from global regions. All these X-ray continua can be well fitted by models consisting of one or two thermal plasmas plus an absorbed power-law. A Gaussian feature is also needed to account for line emission in some cases.

Figure 7 (Upper) shows the X-ray spectrum of the southern nucleus of NGC 6240. A model including thermal plasma emission with $kT\sim$ 0.9 keV plus an absorbed power-law and a Gaussian line is fitted to the data. The bottom panel of Figure 7 shows the global spectral fitting of Arp 299, which can be well described by a thermal plasma with $kT\sim$ 0.7 keV and an absorbed power-law with photon index $\sim$2.

4.2 The Faint Sources

The remaining galaxy nuclei do not have enough counts for the spectral fitting procedure; these sources have total counts ranging from 9 to 69 in 0.3–8.0 keV. Here we use the hardness ratios to estimate their spectral model parameters and fluxes of these faint sources (Teng et al. 2005). Hardness ratio is defined as $HR = (H - S)/(S + H)$, where H and S correspond to the number of counts in the 2.0–8.0 and 0.5–2.0 keV bands, respectively. The hardness ratios obtained from the data can be compared with the hardness ratios produced from the models to determine the model parameters. We have assumed two models – an absorbed power-law and an absorbed single temperature MEKAL. For an absorbed power-law, the power-law index is fixed whereas the column density and temperature (kT) are varied in the MEKAL model. For every model parameter (kT or Γ) and column density set, a model spectrum is generated by XSPEC task FAKEIT. Therefore, the output model spectrum can then be compared with the observational spectrum.

We use these simulated data to calculate the hardness ratio as a function of Γ and $N_{\rm H}$ or kT and $N_{\rm H}$. Values of the model parameters that correspond to the observed hardness ratios are listed in Table 3. Hardness ratios can be a rough indicator of the X-ray spectral properties. As we can see from Table 3, seven of nine sources have a hardness ratio < 0, which indicates the softness of their spectra. By assuming an intrinsic spectral shape, we can estimate $N_{\rm H}$ from the observed spectra. In doing so, we fix the photon index of the power-law at 1.8 which is a typical value for an unabsorbed AGN. The results are listed in the eighth column of Table 3. None of these sources seem to be absorbed by very large column densities. The possible reason is that over rather large nuclear regions of several kpc scales selected for enough X-ray photon counts in the spectral fitting, the average column density of absorption is not necessarily so extreme even though the absorption could be very large in the immediate vicinity of the AGN on a tens or even hundreds of pc scale.

There are still four nuclear sources (IRAS 00188–0856 W, IRAS 03521+0028 E, IRAS 03521+0028 W, IRAS 08572–3915 SE) that do not show obvious (lower than $3\,\sigma$ detection limit) X-ray emissions, so we derive $3\,\sigma$ non-detection upper limits of the count rates. We used the CIAO package PIMMS to convert the count rates to X-ray fluxes and luminosities assuming Galactic absorption and a power-law model with $\Gamma = 1.8$. The fluxes and luminosities of sources are listed in Table 4.

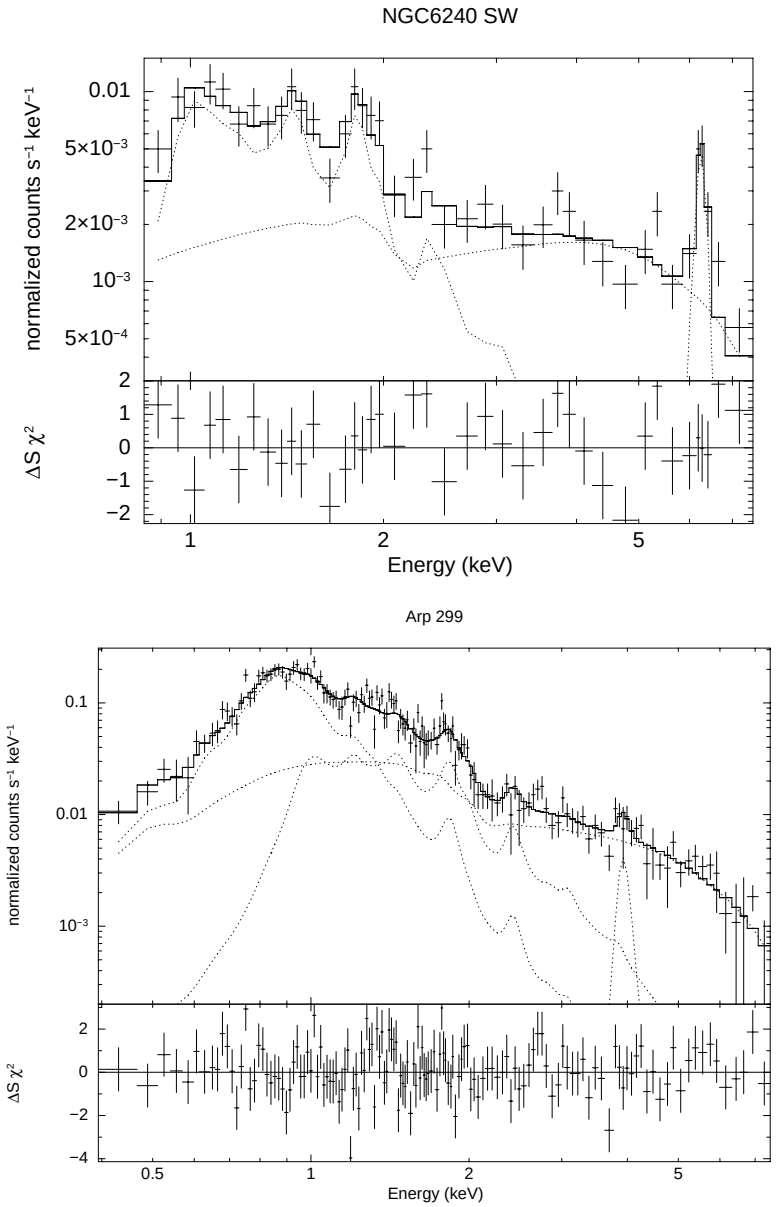

Fig. 7 Nuclear spectrum of southwestern nucleus of NGC 6240 (*upper*); Global spectrum of Arp 299 (*bottom*).

5 DISCUSSION

5.1 General Properties of the Sample

Those nearby galaxies ($z < 0.03$) in our sample often show extended diffuse soft X-ray emission. Hard X-ray emission of all sources in our sample is usually concentrated in the central regions of

Table 3 Spectral Parameters Derived from Hardness Ratios

Source Name	Total Counts	Hard Counts (H)[a]	Soft Counts (S)[a]	Hardness Ratio (HR)[a]	kT[c] keV	$N_{\rm H}$ (10^{22} cm^{-2})	$N_{\rm H}(\Gamma^b = 1.8)$ (10^{22} cm^{-2})
(1)	(2)	(3)	(4)	(5)	(6)	(7)	(8)
IRAS 00188–0856 N	13	6±2.8	7±2.7	–0.08±0.18	$2.1^{+1.7}_{-0.9}$	$0.21^{+0.13}_{-0.20}$	0.28^{+24}_{-0}
IRAS 08572+3915 NW	9	8±3.1	1±0.6	0.78±0.16	$0.6^{+1.5}_{-0.4}$	$9.4^{+4.8}_{-4.3}$	$3.44^{+4.65}_{-2.96}$
IRAS 14348–1447 SW	10	3±1.4	7±2.1	–0.40±0.17	$3.2^{+7.5}_{-2.0}$	$0.17^{+0.42}_{-0.09}$	0.72^{+49}_{-54}
IRAS 14348–1447 NE	15	12±3.5	2±1.4	–0.73±0.14	$2.3^{+4.2}_{-0.9}$	$0.13^{+0.22}_{-0.05}$	0.32^{+49}_{-21}
NGC 7592 E	36	16±4.2	20±4.3	–0.11±0.08	72^{+28}_{-57}	$0.23^{+0.09}_{-0.14}$	0.15^{+31}_{-0}
NGC 7592 W	69	19±4.5	50±5.2	–0.44±0.05	$3.9^{+2.5}_{-1.4}$	$0.24^{+0.25}_{-0.16}$	0.12^{+26}_{-0}
PKS B1345+125 SE	50	40±6.3	10±3.1	0.60±0.06	100^{+0}_{-47}	$0.42^{+0.33}_{-0.27}$	$4.42^{+2.13}_{-0.97}$
III Zw 035 NE	29	13±3.4	16±3.6	–0.12±0.11	$4.8^{+17}_{-2.7}$	$0.38^{+0.25}_{-0.27}$	0.35^{+61}_{-27}
III Zw 035 SW	18	7±1.6	11±2.3	–0.22±0.06	9.1^{+18}_{-6}	$0.23^{+0.17}_{-0.14}$	0.21^{+19}_{-0}

[a] The errors of hardness ratios were determined from error propagation based on the soft and hard band counts.

[b] Γ is the photon index for a power-law model where A(E)=KE$^{\Gamma}$.

[c] The plasma temperature in a MEKAL model. The temperature has an upper limit of $kT = 100$ keV in the MEKAL model.

these galaxies. As mentioned above, most of the bright nuclear cores in this sample need at least two components to fit their spectra. The soft X-ray spectra of six galactic cores show that the hot gas with $kT \sim 0.7$ keV is present. In this aspect, they are very similar to nearby starburst galaxies (Martin et al. 2002). There is a power-law component in every spectral fit which accounts for nearly all the hard X-ray we observed. If the hard X-rays originate from an AGN, then the AGN might be either mostly unabsorbed (hence a low intrinsic luminosity) or absorbed by a very large column density (then most likely it is Compton-thick and detected little by Chandra). All the global spectra of these galaxies in the continuum can be fitted by one or two thermal plasma components with $kT \sim$ 0.3–0.9 keV and a power-law component. The thermal plasma components account for most X-ray emission below $\sim$ 1 keV. However, the power-law model dominates the X-ray emission above ~ 2 keV. The observed hard X-rays may, in principle, originate from either an AGN or a starburst or both.

Arp 299 may be such a galaxy which has both a luminous heavily obscured AGN and a low luminosity AGN. BeppoSAX observations unveiled for the first time a strong yet heavily enshrouded AGN in this system ($N_{\rm H} \simeq 10^{24}$ cm^{-2}, with an intrinsic X-ray luminosity $L_{0.5-100\,{\rm keV}} = 1.9 \times 10_{43}$ erg s^{-1}, Della Ceca et al. 2002). Moreover, *Chandra* and XMM-Newton observations have detected Fe Kα in both the nuclei of IC 694 and NGC 3690 (Ballo et al. 2004). However, the total 2–10 keV luminosities of the nuclei for IC 694 and NGC 3690 are about one order-of-magnitude smaller than the global luminosities of the two galaxies as given in Ballo et al. (2004). The most plausible explanation of X-ray data is the existence of an AGN in each galaxy: one luminous AGN and a low luminosity AGN in the other (Ballo et al. 2004; Zezas et al. 2003). There may be many more similar systems such as Arp 299 in our sample. However, given the much greater distances in comparison, neither the observed exposure time nor the covered hard X-ray band is sufficient to reveal their true nature of possible double-AGNs. Future further deep and hard X-ray (> 10 keV) observations are needed to better constrain their properties.

The observed and absorption-corrected fluxes and luminosities of the nuclear sources in soft (0.5–2.0 keV) and hard X-ray (2.0–10.0 keV) bands are summarized in Table 4, derived from the hardness ratios and spectral fits to the nuclear regions. As our results show that these nuclear sources are usually not absorbed by large column densities, the absorption-corrected fluxes and luminosities are similar to the observed fluxes and luminoisties. Whereas molecular gas with very high column densities are observed in the nuclei of some sources (Downes & Solomon 1998; Bryant & Scoville

Table 4 X-Ray Fluxes and Luminosities of Nuclear Regions

Galaxy Name	Counts[a]	Observ. $S_{0.5-2\mathrm{keV}}$	Unabsorb. $S_{0.5-2\mathrm{keV}}$	Observ. $S_{2-10\mathrm{keV}}$	Unabsorb. $S_{2-10\mathrm{keV}}$	Observ. $L_{0.5-2\mathrm{keV}}$	Unabsorb. $L_{0.5-2\mathrm{keV}}$	Observ. $L_{2-10\mathrm{keV}}$	Unabsorb. $L_{2-10\mathrm{keV}}$
(1)	(2)	(3)	(4)	(5)	(6)	(7)	(8)	(9)	(10)
Arp 220	491±17	1.6E−14	1.6[b]	2.5E−14	13.0[b]	1.0E+40	1.0[b]	1.6E+40	8.0[b]
Arp 299 E	215±12	1.8E−14	2.0	1.4E−13	1.5	3.4E+39	3.9	2.7E+40	2.8
Arp 299 W	267±15	5.3E−14	5.3	2.7E−14	2.8	1.1E+40	1.1	5.4E+39	5.5
IRAS 00188−0856 N	13±4	2.9E−15	2.9	2.6E−14	2.6	8.5E+40	8.5	8.5E+41	8.5
IRAS 00188−0856 S[c]	1±1	1.5E−15	1.5	1.3E−15	1.3	5.2E+40	5.2	5.1E+40	5.1
IRAS 03521+0028 E[c]	3±2	1.2E−15	1.2	1.8E−15	1.8	6.9E+40	6.9	8.6E+40	8.6
IRAS 03521+0028 W[c]	—	1.4E−15	1.4	3.0E−15	3.0	8.2E+40	8.2	1.7E+41	1.7
IRAS 08572+3915 NW[c]	12±3	6.2E−16	25.4	4.0E−14	4.0	3.3E+39	18.1	2.6E+41	2.6
IRAS 08572+3915 SE	—	4.8E−16	4.8	3.0E−14	3.0	2.8E+39	2.8	2.0E+41	2.0
IRAS 14348−1447 NE	17±4	3.4E−15	3.4	8.2E−15	8.2	4.6E+40	4.6	1.2E+41	1.2
IRAS 14348−1447 SW	27±5	6.0E−15	6.0	3.7E−15	3.7	8.4E+40	8.4	5.8E+40	5.8
Mrk 266 NE	343±18	3.8E−14	4.1	2.7E−13	2.7	5.8E+40	6.0	4.2E+41	4.2
Mrk 266 SW	144±12	2.6E−14	2.6	2.0E−14	2.0	4.1E+40	4.1	3.1E+40	3.1
Mrk 273	1038±29	2.6E−14	4.0	5.0E−13	5.0	7.4E+40	11.5	1.5E+42	1.5
Mrk 463 E	1216±34	5.0E−14	5.0	2.8E−13	2.8	2.6E+41	2.6	1.5E+42	1.5
Mrk 463 W	292±17	9.0E−15	9.0	2.8E−13	2.8	4.8E+40	4.8	1.3E+42	1.3
NGC 6240 NE	586±24	1.6E−14	1.8	4.9E−13	4.9	1.8E+40	1.9	5.8E+41	5.8
NGC 6240 SW	670±26	2.9E−14	3.3	4.8E−13	4.8	3.4E+40	4.4	5.1E+41	5.1
NGC 7592 E	36±8	4.9E−15	6.0	3.3E−14	3.3	6.7E+39	8.2	3.8E+40	3.8
NGC 7592 W	69±10	1.9E−14	1.9	4.0E−14	4.0	2.2E+40	2.2	4.7E+40	4.7
PKS B1345+125 NW	1060±33	4.6E−14	4.6	6.6E−13	7.7	1.0E+42	1.0	2.3E+43	2.6
PKS B1345+125 SE	50±9	2.1E−15	3.0	4.8E−14	7.9	5.1E+40	7.2	1.7E+42	3.2
VV 114 E	453±17	2.1E−14	2.1	2.5E−14	12.7	1.7E+40	1.7	2.0E+40	9.7
VV 114 W	389±18	1.3E−14	1.3	6.3E−14	6.8	5.2E+39	6.1	5.4E+39	6.6
III Zw 035 NE	29±7	3.3E−15	3.6	2.8E−16	2.8	4.7E+39	5.4	3.6E+40	3.6
III Zw 035 SW	18±6	2.1E−15	2.3	1.6E−14	1.6	2.9E+39	9.2	2.4E+40	2.4

[a] Total net counts used in spectral fitting.

[b] The same magnitude as the observed fluxes or luminosities of the sources.

[c] 2 σ non-detection upper limits of fluxes and luminosities.

Note: Fluxes and luminosities are in units of erg cm^{-2} s^{-1}. The second column is the photon counts. The 3th, 4th, 5th and 6th columns are the flux of those sources. The last four columns are the luminosities of these sources.

1999), these molecular gas concentrations are usually extremely compact. The area we selected in our X-ray spectral analysis is much larger in order to have enough X-ray photon counts, and thus the average absorption over such an extended area is much smaller. Part of the photon index is very small and/or even negative, which may also indicate strong absorption.

In fact, the measurements of N_{H} in AGNs are sometimes more complicated than modeling with an absorbed power-law (or an absorbed power-law plus a plasma model), mostly due to the contamination from the host galaxy, scattering component, and reflection component. The contribution from the host galaxy is not limited to plasma emission, but also includes a power-law component. For example, Brightman & Nandra (2008) showed that there are many cases where heavily obscured X-ray AGNs could be misclassified as little absorption or unobscured through X-ray spectral fitting.

Our *Chandra* archive study shows that these (U)LIRGs are very faint in X-rays compared with the AGNs of comparable bolometric and/or IR luminosities. The measured X-ray luminosities of most sources are lower than 10^{42} erg s^{-1}, even if their total IR outputs are always larger than $\sim 10^{45}$ erg s^{-1}. However, these sources are still bright as compared to nearby low luminosity AGNs

(LLAGN, Jimenez-Bailon et al. 2007), even though this possibility would not have an essential impact on the total energy outputs of the entire galaxies.

5.2 Implication of X-ray Images/Spectra

As mentioned above, we find that these "AGN" nuclei are more luminous than the other nuclei in the four galaxies. There may be two explanations for this phenomenon. One explanation is that the intrinsic X-ray emissions of these "AGN" nuclei are stronger than these "H II" nuclei. However, these "H II" may be heavily absorbed and possess an AGN which is misclassified by former optical and even IR observations. Jiménez-Bailón et al. (2007) report strong evidence of AGNs in a galaxy pair which was previously classified as H II galaxies. Mrk 266 may be an additional candidate to a binary AGN since both of the nuclei of Mrk 266 have been detected in the hard X-ray band, and other multi-band observations indicate that both can be classified as an AGN. This source can be a good candidate of a binary AGN. However, the X-ray luminosites of the two nuclei and the upper limit of Fe-K luminosites are rather low. The northeastern nucleus exhibits a very flat power law, which probably suggests that this source is heavily absorbed.

5.3 X-ray vs. Far-Infrared

Following Ptak et al. (2003), we plot the ratios of hard X-ray to far-infrared fluxes as a function of the infrared luminosities and the $\frac{F_{25\,\mu\mathrm{m}}}{F_{60\,\mu\mathrm{m}}}$ flux ratio (Fig. 8).This IRAS 25 to 60 μm flux ratio is a measure of luminosity-weighted mean dust temperature and a useful empirical diagnostic to assess the relative energetic importance of starburst and AGN activities in a galaxy (de Grijp et al. 1987). Compared with samples of galaxies observed with ASCA (Dahlem et al. 1998; Della Ceca et al. 1996, 1999; Moran et al. 1999; Ptak et al. 1999; Turner et al. 1997), our results are consistent with Ptak et al. (2003) and Teng et al. (2005) since both the ratios of the hard X-ray to far-infrared and the infrared colors are generally similar to those pure starburst galaxies, suggesting that most galaxies in our sample are powered by starburst though all galaxies in our sample have an AGN signature in optical and infrared bands, including at least three (U)LIRGs with a known binary AGN.

According to Boller & Bertoldi (1996) and Boller et al. (1998), the flux ratio of soft X-ray (0.1–2.4 keV, ROSAT) to far-infrared is $10-1$ for unabsorbed Seyfert 1 galaxies and $10^{-2.5}$ for an unabsorbed starburst galaxy. The ratio is a good indicator of the main energy source of ULIRGs (Xia et al. 2001). We scale the 0.5–2.0 keV fluxes to 0.1–2.4 keV based upon the method adopted in Teng et al. (2005) using the photo indexes of the soft power-law continuum model. In Figure 9, we plot the soft X-ray (0.1–2.4 keV) to far-infrared ratio for our sample of galaxies as a function of the infrared luminosities and the 25 to 60 μm flux ratio. All sources in our sample have an X-ray to far-infrared flux ratio lower than $10^{-2.5}$, suggesting the dominant starburst nature of these sources.

5.4 Comparison with Previous Work

The analysis of Chandra observations of 10 sources in our sample has previously been presented (Xia et al. 2002; Clements et al. 2002; McDowell et al. 2003; Komossa et al. 2003; Ptak et al. 2003; Zezas et al. 2003; Ballo et al. 2004; Imanishi & Terashima 2004; Teng et al. 2005; Grimes et al. 2006; Brassington et al. 2007; Bianchi et al. 2008). This study concentrates more on revealing the existence of binary AGNs and the energy sources in these galaxies and presents new X-ray observations of four (U)LIRGs (IRAS 08572+3915, IRAS 14348−1447, NGC 7592, III Zw 035) from the Chandra archive for the first time.

Here we make a rough comparison with those previous results. In our study, we have extracted the spectra of each nucleus (with the exceptions of Arp 220 and Mrk 273), which have not been done by Teng et al. (2005) and Imanishi & Terashima (2004) for IRAS 00188−0856, IRAS 03521+0028,

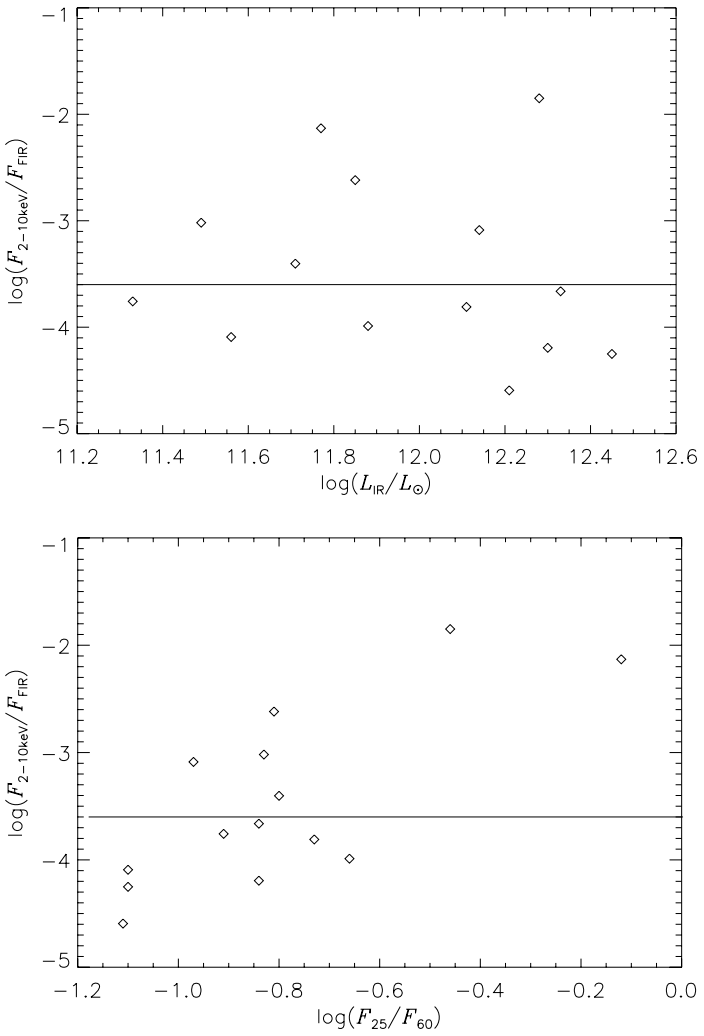

Fig. 8 Plots of the log of the ratio of hard X-ray (2.0–10 keV) to far-infrared flux against the log of the 25 μm to 60 μm flux ratio and the log of the infrared luminosity.

and PKS 1345+125. Thus, spectral analysis is new for a total of 7 (U)LIRGs – half of our sample. We have also fitted each nuclear spectrum with the MEKAL plasma+power-law+gaussian line model, and all of the fits give us acceptable χ^2/dof values. While various models have been used in previous studies of these sources, which further caused the difference in the fluxes and luminosities to a certain extent with those former results, our specific efforts of focusing on the double-nucleus are by far the most uniform and systematic study of such a topic.

Chandra observations cannot fully resolve the double-nucleus of Arp 220 and Mrk 273 because both of them have very small nuclear separations ($\sim 1''$, Scoville et al. 2000; Tacconi et al. 2002). Nevertheless, Xia et al. (2002) and Iwasawa et al. (2001) reported strong evidence for the presence of an AGN in Mrk 273 and Arp 220 respectively. Therefore, there is still a possibility for the presence of binary AGNs in the two galaxies.

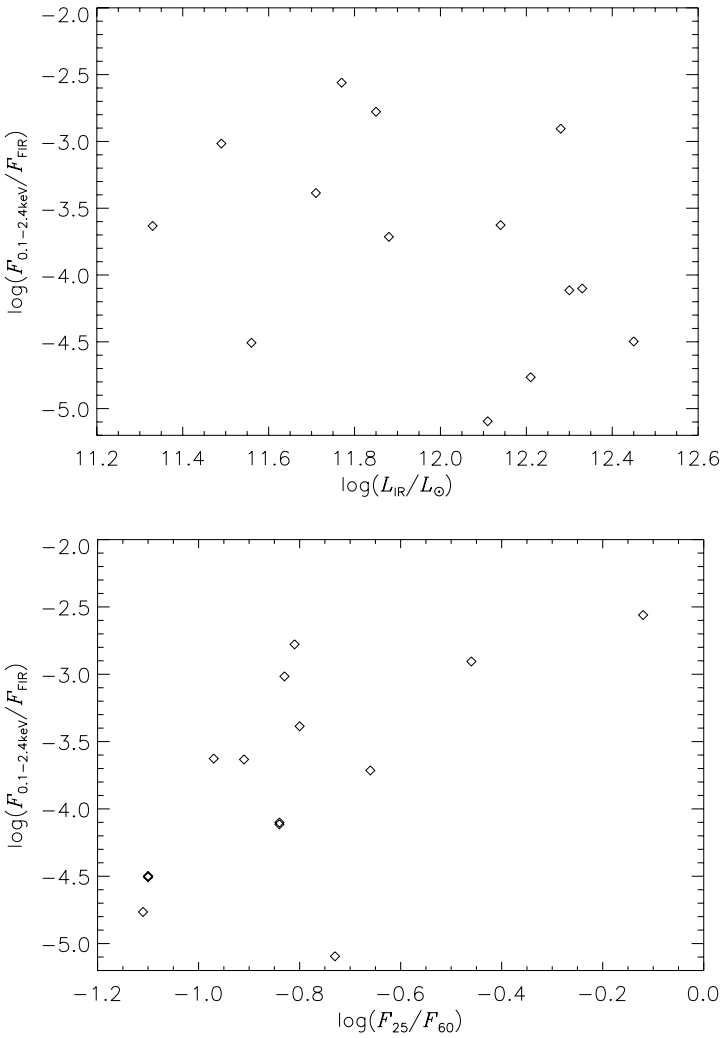

Fig. 9 Plots of the log of the ratio of 0.1–2.4 keV to far-infrared flux against the log of the 25 μm to 60 μm flux ratio and the log of the infrared luminosity.

6 SUMMARY

We have analyzed the *Chandra*/ACIS X-ray observations from the *Chandra* archive of 14 (U)LIRGs with a double-nucleus with at least one of the double-nuclei showing an AGN signature; these galaxies are good candidates for possessing binary AGNs. This paper makes an important effort in specifically searching for binary AGNs from a large sample of merging (U)LIRGs. Except for one non-detection in X-ray given the limited short exposure, 13 out of 14 (U)LIRGs are detected in the 0.5–8.0 keV energy band. We find that the measured X-ray luminosities of these sources are on average smaller than 10^{42} erg s^{-1}, which confirms that (U)LIRGs are potentially faint X-ray sources. The soft and hard X-ray to far-infrared flux ratios suggest that most galaxies in our sample are not

energetically dominated by AGNs. A thermal component with $kT \sim 0.7$ keV is present in seven nuclear cores, which may be associated with a nuclear or circumnuclear starburst.

Mrk 266 may be an additional candidate for binary AGNs since both nuclei are detected in hard X-ray and have been classified as an AGN from other studies even though there is no direct indication of AGNs in the 0.3–10 keV band. Nine (U)LIRGs are found to have X-ray counterparts to their double nuclei in optical and near-infrared images, including three previously studied (U)LIRGs with known binary AGNs and Mrk 266. In the other non-binary AGNs, the "AGN" nuclei are usually more luminous than the other nuclei of the galaxies in two merging (NGC 7592, PKS B1345+125) pairs, whereas the other three merging pairs (IRAS 14348−1447, III Zw 035, VV 114) are comparable. These are new X-ray observations first reported here except for PKS B1345+125. In the other 4 (U)LIRGs, two previously studied ULIRGs (Arp 220 and Mrk 273) are spatially unresolved in X-ray; another two have only one obvious X-ray counterpart to the double-nucleus as the other component of the pair is not detected in X-ray. Most AGN sources in our sample are quite faint in X-ray and the energetic AGN with strong hard X-ray emission is rather rare.

We have extracted the nuclear and global spectra for each of the nuclei, but only about half of the nuclear spectra are bright enough for conventional spectral fitting. The remaining ones are too faint to have significant counts for a traditional spectral fitting. We use the hardness ratios to estimate the spectral parameters of the faint sources. Our analysis shows that the X-ray emission of most galaxies in our sample is not dominated by an AGN, due to both the lack of an Fe K line detected and the weak emission in hard X-ray band (2–10 keV) in these sources. We conclude that our study does not provide newly confirmed examples of binary AGNs. However, we cannot exclude the possibility that binary AGNs, which have a low intrinsic luminosity or are obscured by a large column density of gas/dust, exist in all of our samples, particularly for the highly obscured and spatially unresolved systems. Hard (> 10 keV) X-ray observations with high resolution are needed to place more constraints on the presence of AGNs in these galaxies.

Acknowledgements We are grateful to the anonymous referee for the careful readings and useful suggestions in the referee reports that helped improve the presentation of this paper. Research for this project is supported by the National Natural Science Foundation of China (Distinguished Young Scholars, Grant Nos. 10425313, 10833006 and 10621303), Chinese Academy of Sciences' Hundred Talent Program, and 973 project of the Ministry of Science and Technology of China (Grant No. 2007CB815406).

References

Arnaud, K. A. 1996, Astronomical Data Analysis Software and Systems V, 101, 17
Ballo, L., Braito, V., Della Ceca, R., Maraschi, L., Tavecchio, F., & Dadina, M. 2004, ApJ, 600, 634
Bender, P. L. 1998, Bulletin of the American Astronomical Society, 30, 1326
Bianchi, S., Chiaberge, M., Piconcelli, E., Guainazzi, M., & Matt, G. 2008, MNRAS, 386, 105
Boller, T., & Bertoldi, F. 1996, The Physics of Liners in View of Recent Observations, 103, 159
Boller, T., Bertoldi, F., Dennefeld, M., & Voges, W. 1998, A&AS, 129, 87
Brassington, N. J., Ponman, T. J., & Read, A. M. 2007, MNRAS, 377, 1439
Brightman, M., & Nandra, K. 2008, MNRAS, 390, 1241
Britzen, S., Roland, J., Laskar, J., Kokkotas, K., Campbell, R. M., & Witzel, A. 2001, A&A, 374, 784
Bryant, P., & Scoville, N. 1999, AJ, 117, 2632
Clements, D. L., McDowell, J. C., Shaked, S., Baker, A. C., Borne, K., Colina, L., Lamb, S. A., & Mundell, C. 2002, ApJ, 581, 974
Dahlem, M., Weaver, K., & Heckman, T. 1998, ApJS, 118, 401
de Grijp, M. H. K., Lub, J., & Miley, G. K. 1987, A&AS, 70, 95

Della Ceca, R., Griffiths, R., Heckman, T., & MacKenty, J. 1996, ApJ, 469, 662
Della Ceca, R., et al. 2002, ApJ, 581, L9
Della Ceca, R., Griffiths, R., Heckman, T., Lehnert, M., & Weaver, K. 1999, ApJ, 514, 772
Dickey, J. M., & Lockman, F. J. 1990, ARA&A, 28, 215
Dopita, M. A., Pereira, M., Kewley, L. J., & Capaccioli, M. 2002, ApJS, 143, 47
Downes, D., & Solomon, P. M. 1998, ApJ, 507, 615
Evans, D. A., et al. 2008, ApJ, 675, 1057
Franceschini, A., et al. 2003, MNRAS, 343, 1181
Haehnelt, M. G., & Kauffmann, G. 2002, MNRAS, 336, L61
Gaskell, C. M. 1985, Nature, 315, 386
Genzel, R., Lutz, D., Sturm, E., Egami, E., Kunze, D., Moorwood, A. F. M., Rigopoulou, D., Spoon, H. W. W., Sternberg, A., Tacconi-Garman, L. E., Tacconi, L., & Thatte, N. 1998, ApJ, 498, 579
Grimes, J. P., Heckman, T., Hoopes, C., Strickland, D., Aloisi, A., Meurer, G., & Ptak, A. 2006, ApJ, 648, 310
Guainazzi, M., Piconcelli, E., Jiménez-Bailón, E., & Matt, G. 2005, A&A, 429, L9
Imanishi, M., & Terashima, Y. 2004, AJ, 127, 758
Iwasawa, K., Matt, G., Guainazzi, M., & Fabian, A. C. 2001, MNRAS, 326, 894
Jiménez-Bailón, E., Loiseau, N., Guainazzi, M., Matt, G., Rosa-González, D., Piconcelli, E., & Santos-Lleó, M. 2007, A&A, 469, 881
Joseph, R. 1999, Ap&SS, 266, 321
Kim, D.-C., & Sanders, D. B. 1998, ApJS, 119, 41
Komossa, S., Burwitz, V., Hasinger, G., Predehl, P., Kaastra, J. S., & Ikebe, Y. 2003, ApJ, 582, L15
Lauer, T. R., et al. 2002, AJ, 124, 1975
Le Floc'h, E., et al. 2002, A&A, 391, 417
Lira, P., Ward, M., Zezas, A., Alonso-Herrero, A., & Ueno, S. 2002, MNRAS, 330, 259
Martin, C. L., Kobulnicky, H. A., & Heckman, T. M. 2002, ApJ, 574, 663
Mazzarella, J. M., Gaume, R. A., Aller, H. D., & Hughes, P. A. 1988, ApJ, 333, 168
McDowell, J. C., et al. 2003, ApJ, 591, 154
Merritt, D. 2001, ApJ, 556, 245
Merritt, D. 2002, ApJ, 568, 998
Moran, E., Lehnert, M., & Helfand, D. 1999, ApJ, 526, 649
Ptak, A., Serlemitsos, P., Yaqoob,T., Mushotzky, R. 1999, ApJS, 120, 179
Ptak, A., Heckman, T., Levenson, N. A., Weaver, K., & Strickland, D. 2003, ApJ, 592, 782
Roos, N., Kaastra, J. S.,& Hummel, C. A. 1993, ApJ, 409, 130
Rossa, J., Laine, S., van der Marel, R. P., Mihos, J. C., Hibbard, J. E., Böker, T., & Zabludoff, A. I. 2007, AJ, 134, 2124
Sanders, D., & Mirabel, I. 1996, ARA&A, 34, 749
Sanders, D. 1999, Ap&SS, 266, 331
Sanders, D. B., Mazzarella, J. M., Kim, D.-C., Surace, J. A.,& Soifer, B. T. 2003, AJ, 126, 1607
Schoenmakers, A. P., de Bruyn, A. G., Röttgering, H. J. A., & van der Laan, H. 2000, MNRAS, 315, 395
Scoville, N. Z., et al. 2000, AJ, 119, 991
Tacconi, L. J., Genzel, R., Lutz, D., Rigopoulou, D., Baker, A. J., Iserlohe, C., & Tecza, M. 2002, ApJ, 580, 73
Taniguchi, Y., & Wada, K. 1996, ApJ, 469, 581
Teng, S. H., Wilson, A. S., Veilleux, S., Young, A. J., Sanders, D. B., & Nagar, N. M. 2005, ApJ, 633, 664
Thorne, K. S., & Braginskii, V. B. 1976, ApJ, 204, L1
Turner, T., George, I., Nandra,K., & Mushotzky, R. 1997, ApJS, 113, 23
Valtaoja, E., Teräsranta, H., Tornikoski, M., Sillanpää, A., Aller, M. F., Aller, H. D., & Hughes, P. A. 2000, ApJ, 531, 744
Veilleux, S., Kim, D.-C., Sanders, D. B., Mazzarella, J. M., & Soifer, B. T. 1995, ApJS, 98, 171
Veilleux, S., Sanders, D. B., & Kim, D.-C. 1997, ApJ, 484, 92

Veilleux, S., Sanders, D. B., & Kim, D.-C. 1999, ApJ, 522, 139
Veilleux, S., Kim, D.-C., & Sanders, D. B. 2002, ApJS, 143, 315
Villata, M., & Raiteri, C. M. 1999, A&A, 347, 30
Wang, T.-G., Zhou, H.-Y., & Dong, X.-B. 2003, AJ, 126, 113
Xia, X.-Y., Boller, T., Deng, Z.-G., & Brner, G. 2001, ChJAA (Chin. J. Astron. Astrophys.), 1, 221
Xia, X. Y., Xue, S. J., Mao, S., Boller, T., Deng, Z. G., & Wu, H. 2002, ApJ, 564, 196
Zezas, A., Ward, M. J., & Murray, S. S. 2003, ApJ, 594, L31
Zier, C., & Biermann, P. L. 2001, A&A, 377, 23
Zier, C., & Biermann, P. L. 2002, A&A, 396, 91
Zink, E. C., Lester, D. F., Doppmann, G., & Harvey, P. M. 2000, ApJS, 131, 413
Zhou, H., Wang, T., Zhang, X., Dong, X., & Li, C. 2004, ApJ, 604, L33